Atmos. Chem. Phys. Discuss., 11, 2655–2696, 2011
www.atmos-chem-phys-discuss.net/11/2655/2011/
doi:10.5194/acpd-11-2655-2011

Atmospheric Chemistry and Physics Discussions

Organic functional groups in aerosol particles from burning and non-burning forest emissions at a high-elevation mountain site

S. Takahama[1], R. E. Schwartz[1], L. M. Russell[1], A. M. Macdonald[2], S. Sharma[2], and W. R. Leaitch[2]

[1]Scripps Institution of Oceanography, University of California San Diego, La Jolla, CA, USA
[2]Environment Canada, Science and Technology Branch, Toronto, ON, Canada

Received: 12 December 2010 – Accepted: 23 December 2010 – Published: 24 January 2011

Correspondence to: L. M. Russell (lmrussell@ucsd.edu)

Published by Copernicus Publications on behalf of the European Geosciences Union.

Abstract

Ambient particles collected on teflon filters at the Peak of Whistler Mountain, British Columbia (2182 m a.s.l.) during spring and summer 2009 were measured by Fourier transform infrared (FTIR) spectroscopy for organic functional groups (OFG). The project mean and standard deviation of organic aerosol mass concentrations (OM) for all samples was 3.2±3.3 ($\mu g\,m^{-3}$). The OM was dominated by regional forest sources, burning, and non-burning that occurred mostly during June–September. On average, organic hydroxyl, alkane, carboxylic acid, ketone, and amine, groups represented 31%±11%, 34%±9%, 23%±6%, 6%±7%, and 6%±3% of OM, respectively. Ketone groups were associated with the forest aerosols and represented up to 27% of the OM in these aerosols. Additional measurements of aerosol mass fragments, size, and number concentrations were used to separate fossil-fuel combustion and burning and non-burning forest sources of the measured organic aerosol. The OM concentrations observed at Whistler Peak during this campaign were higher than those measured during a shorter period in the spring of 2008 at a site in Whistler valley, over one km lower than the peak location. The 2009 campaign was largely influenced by the wildfire emissions that were absent during the 2008 campaign.

1 Introduction

Burning and non-burning forest emissions are important contributors to primary and secondary organic mass (OM) (Bond et al., 2004; Hallquist et al., 2009). Bond et al. (2004) name biomass burning (BB) as the largest (42%) combustion source of primary organic carbon, outweighing both fossil fuel (38%) and biofuel (20%) combustion, and accounting for 31 to 45 $Tg\,C\,yr^{-1}$ of the global primary organic aerosol (POA). Gas phase compounds also result in significant aerosol formation (secondary organic aerosol, SOA). Globally, biogenic volatile organic compounds (BVOCs) emissions may be 10 times greater than anthropogenic VOC emissions (Seinfeld and Pandis, 2006).

ACPD
11, 2655–2696, 2011

Oxidation of BVOCs yields a large biogenic contribution to SOA, with estimates ranging from 12 to 70 Tg C yr^{-1} (Hallquist et al., 2009).

These significant forest-related emissions present a complex issue for climate science and climate prediction due to a number of possible feedbacks. Large uncontrollable fires are expected to increase with climate change (IPCC, 2007) due to reduced rainfall and increased temperatures. Bowman et al. (2009) discuss how fires in turn influence climate due to their large greenhouse gas (CO_2 emissions equal to 50% of those from fossil fuel combustion) and aerosol particle (40% of black carbon, along with large POA emissions discussed) emissions. Kulmala et al. (2004) explores feedbacks between climate and non-burning forest emissions. They present evidence that increased temperatures and CO_2 concentrations will act to fertilize forests, which will in turn create a large BVOC source and ultimately result in a cooling effect from the increased biogenic aerosol.

The radiative impacts of aerosol particles are altitude-dependent (Penner et al., 2003). Chuang et al. (2002) estimated the forcing from the first indirect effect associated with organic aerosol from BB to be $-1.16\,W\,m^{-2}$. Injection of aerosol particles higher in the atmosphere can increase particle lifetime and thus the ability to influence climate. Higher-altitude injections of organic BB aerosol may absorb longwave radiation, leading to negative forcing (Penner et al., 2003). Additionally, global chemical transport models have been reported to under-predict organic aerosol in the free troposphere by 10–100 times when compared to ambient measurements (Heald et al., 2005) during the ACE-Asia campaign (NW Pacific, 2001), though reported model-measurement discrepancies were much lower when large contributions from biomass burning and biogenic SOA were simulated for the ICARTT campaign measurements (NE North America, 2004) (Heald et al., 2006).

In this study, we use ambient measurements and statistical techniques to characterize organic functional groups (OFG) associated with aerosols from both burning and non-burning forest emissions at a lower free troposphere, high-elevation mountain site in Whistler, British Columbia, in spring and summer 2009.

ACPD
11, 2655–2696, 2011

2 Methods

Since 2002, Environment Canada (EC) has conducted atmospheric composition measurements at Whistler Peak in the lower troposphere (2182 m a.s.l.) (Macdonald et al., 2006). One of the many objectives of the site is to monitor changes in the composition and concentration of particulate pollutants entering North America from Asia, document the aerosol in the free troposphere, and study the forest aerosol. The present sampling campaign consists of measurements from 26 March 2009 to 27 April 2009 (first sampling period) and 23 May 2009 to 10 September 2009 (second sampling periods). The break in between was due to a logistical interruption in operations.

Atmospheric particles were sampled on teflon filters and analyzed by Fourier transform infrared (FTIR) spectroscopy and X-ray fluorescence (XRF) techniques for organic functional groups (OFG) and elemental composition. FTIR spectroscopy provides OFG concentrations, including alkane, carboxylic acid, organic hydroxyl, amine, ketone, alkene, and aromatic groups, through chemical bond-based measurements in atmospheric particles collected on a substrate (Russell et al., 2009). Over a sampling period of approximately three days, five filter samples were collected, with three measurements collected simultaneously on 37 mm Teflon filters (Pall Inc.). The filter collection was divided by size into total and submicron filters, and by day and night samples with an automated switch occurring at 06:30 a.m. and 06:30 p.m. PST daily. The total samples were collected from an inlet with no size-selection. Total samples can be considered to include collection of particles up to 10 µm with the absolute upper limit dependent on ambient conditions, such as wind speed and precipitation. Submicron samples were collected downstream of a 1 µm impactor (Brechtel Manufacturing, Inc., Hayward, CA). A full-day filter type (sampling through both day and night) was changed from having a submicron to total sizecut on 29 May 2009. The filters were sampled in a refrigerator at ca. 4 °C to reduce losses from volatilization over the multiple day exposure period. Samples were kept frozen until analysis by FTIR spectroscopy. The filters were equilibrated in a temperature and humidity-controlled cleanroom environment for

ACPD
11, 2655–2696, 2011

24 h before FTIR spectroscopic analysis. FTIR sample spectra were measured with a Tensor 27 spectrometer (Bruker, Billerica, MA), and baselined and fitted with peaks to identify OFG using the method described by Russell et al. (2009). Alkene, aromatic, and organonitrate groups were below detection limit for all samples. Organosulphate groups were above detection limit during only one three day-long sampling period. XRF analysis provides quantitative measurements of elemental composition. 90 of the same filter samples used for FTIR, the majority of which are submicron samples, were sent to Chester LabNet (Tigard, Oregon) for elemental analysis of elements Na and heavier (Maria et al., 2003).

Scanning Transmission X-Ray Microscopy with Near-Edge X-Ray Absorption Fine Structure (STXM-NEXAFS; Stöhr, 1992) with processing algorithms described by Takahama et al. (2010) was also used to examine single particle morphology and composition for a limited number of particles. With this method, X-rays generated at the Advanced Light Source at Lawrence Berkeley National Laboratories (Beamline 5.3.2) are used to probe the electronic structure of individual particles at a spatial resolution of approximately 30 nm. Collectively, 30 particles from samples collected on 1 August 16:30 and 21 August 16:30 2009, were analyzed as allowed by our beamtime allocation.

Particle number concentrations were measured using a TSI 3025 Ultrafine Condensation Particle Counter (UCPC) throughout the study. Particle size distributions from 0.01 to 0.5 µm diameter were measured with a MSP Wide-range Particle Spectrometer (WPS; Liu et al., 2010) until 28 June and a TSI 3034 Scanning Mobility Particle System (3034-SMPS) from 1–31 August; malfunctions terminated measurements in both cases. The WSP contains a Scanning Mobility Spectrometer (SMS) for particle measurement from 0.01 to 0.5 µm and a Laser Particle Spectrometer (LPS) for measurement in the 0.5 to 10 µm range. Despite the malfunction of the SMS on June 28, the LPS continued to operate and particle size distributions from 0.5 to 10 µm were measured with the LPS throughout the study period. The LPS data are based on the manufacturer's calibration using polystyrene latex particles (PSLs; real refractive index

ACPD
11, 2655–2696, 2011

of 1.585), but here we only use the data to estimate the number concentrations of supermicron particles. The SMS and the 3034-SMPS measurements are based on particle mobility in an electric field. Sizing by the SMS and 3034-SMPS was verified on site using nearly monodisperse particles selected with a TSI 3071 Electrostatic Classifier calibrated with PSLs. Comparisons of 30-min averaged total particle number concentrations from the UCPC with the 3034 during situations when particles were <20 nm diameter are <3% of the total, which included BB aerosols, show the particle concentration measurements agree to within 10% and on average differ by 5%. The same comparison of the SMS and the UCPC indicate the SMS co-varied but was biased low relative to the UCPC by about 20% on average.

An Aerodyne Aerosol Chemical Speciation Monitor (ACSM; Ng et al., 2011) was installed at Whistler Peak in early July 2009. The ACSM is similar to the Aerodyne Aerosol Mass Spectrometer (AMS; Jayne et al., 2000) with the primary differences being no particle time-of-flight measurement and reduced sensitivity. The ACSM uses a Pfeiffer Prisma quadrapole and scans over 150 mass/charge (*m/z*) units. At Whistler Peak, the scan rate is set to 1 *m/z* per second and every other scan is performed on filtered aerosol. The difference between alternate ambient and filter scans (12 scans in total) is averaged over a 30 min period to produce a sample data point. The ACSM uses an internal permeation source of naphthalene, identified at *m/z* 128, to provide the system constant after correction for chamber temperature. Mass calibrations are done with nearly monodisperse particles of ammonium nitrate, and the relative ionisation efficiencies for sulphate and organics are based on the AMS. The data analysis is based on Allan et al. (2004) and Canagaratna et al. (2007). The measured detection limits for the 30 min averaged samples collected at Whistler peak are 40 ng m^{-3} for nitrate, 40 ng m^{-3} for sulphate and 600 ng m^{-3} for the total organic components.

Teflon filters sampled at 16.7 l min^{-1} over successive 48 h periods through a 2.5 µm URG cyclone were analyzed by ion chromatography for ions of chloride, nitrate, sulphate, sodium, ammonium, potassium.

ACPD
11, 2655–2696, 2011

A Droplet Measurement Technologies, Inc. Single Particle Soot Photometer (SP2) was installed at Whistler Peak also in early July. Aerosol particles are sampled into the cavity of a Nd:YAG lasing crystal (1064 nm) where the particles containing black carbon (BC) absorb the energy and thermally irradiate as they vapourize at approximately 4000 K. The emitted thermal radiation (at visible wavelengths) is detected with red and blue sensitive photomultipliers. A comprehensive discussion of the SP2 operation and calibration is given by J. P. Schwarz et al. (2010). A linear calibration curve was generated by SP2 response to particles atomized from "Aquadag" in solution and size selecting them by using a TSI Electrostatic Classifier. The results also indicated a lower size threshold for detection of a BC particle of about 110 nm mobility diameter. PAPI software developed by DMT was used for the data analysis. The details of PAPI software performance and evaluations with other methods have been described Subramanian et al. (2010) and Cross et al. (2010). The details of PAPI software performance and evaluations with other methods have been described by Subramanian et al. (2010) and Cross et al. (2010).

The ambient aerosol particles were delivered into the instrument room through a stainless steel manifold with an open intake covered above by a slightly conical hat. The flow through the 7.3 cm ID manifold is approximately 120 l m^{3}, equivalent to a speed of about 0.5 m s^{-1}. The manifold is about 6 m total length and therefore the average residence time is about 12 s. The transfer time from the manifold to each instrument is <1 s. At the end of the manifold, particles are sampled from near the centre of the flow to minimize wall losses of primarily ultrafine particles. Losses of coarse particles are primarily defined by the horizontal wind speeds at the intake point, and previous comparisons with other measurements suggest that particles of at least 6 µm diameter are sampled with efficiency equivalent to the measurement uncertainty. The intake of the manifold is heated to a minimum of 4 °C in order to prevent riming of the intake when supercooled cloud is present. The aerosol drawn down the manifold into the room housing the instruments is further warmed up to as much as 20 °C. In the case of the filters for the OFG analysis this warming is momentary as the aerosol is

ACPD
11, 2655–2696, 2011

collected onto filters housed in a refrigerator held at a temperature of approximately 4 °C. The sampling line connecting the filters to the manifold was nearly vertical and about 1 m of 1 cm ID stainless steel tubing.

To compare similarity of ambient ACSM mass spectra to reference mass spectra of dark α-pinene ozonolysis (Shilling et al., 2009), we use the cosine angle metric – defined as $\theta = \arccos\left(x^T y / \|x\| \|y\|\right)$ where x and y are ion counts of two spectra (one ambient and the other reference in this case) at m/z units of 43, 44, 57, 60, and 73, represented as vectors. The medium and high VOC loading case (spectrums (ii) and (iii) from Shilling et al., 2009) are used for comparison. This value is also proportional to the Euclidean distance metric between spectra normalized by their respective dot products.

The composition and contribution of multiple components in submicron FTIR spectra were inferred by application of regression analysis and Positive Matrix Factorization (PMF; Paatero and Tapper, 1994) to the spectra matrix consisting of samples and wavenumbers in the two dimensions. PMF has been applied to FTIR spectra to identify and separate varying components (Russell et al., 2009; Hawkins and Russell, 2010; R. E. Schwartz et al., 2010). Solutions using rotation parameter FPEAK of −1.2 to 1.2 by increments of 0.6, seed values of 1, 10, and 100, and number of factors between two to six were examined. The Explained Variation (EV) metric is used to report what fraction or percentage of the variation in a sample spectrum is captured by the PMF components, and is defined as (Paatero, 2007)

$$\mathrm{EV}_{ik} = \frac{\sum_{j=1}^{m} \left| g_{ik} f_{kj} \right| / s_{ij}}{\sum_{j=1}^{m} \left(\sum_{h=1}^{p} \left| g_{ih} f_{hj} \right| + \left| e_{ij} \right| \right) / s_{ij}} \quad \forall\, k = 1, \ldots, p \tag{1}$$

where i is the sample number, k is the factor number, and p is the number of factors chosen. g_{ik} is strength or contribution of factor k to the ith sample, f_{kj} is value (absorbance) of factor k for variable (wavenumber) j, and e_{ij} is the residual as defined in the factor analytic expression, $x_{ij} = \sum_{k=1}^{p} g_{ik} f_{kj} + e_{ij}$, where x_{ij} is the

ACPD
11, 2655–2696, 2011

absorbance for the ith sample at wavenumber j. s_{ij} is the standard deviation matrix (or inverse squared weighting matrix) which is used in the minimization expression, $Q = \sum_{i=1}^{n} \sum_{j=1}^{m} \sum_{j} e_{ij}^2 / s_{ij}^2$, subject to non-negativity constraints on g_{ik} and f_{kj} for n samples and m wavenumbers. A lack of differences among the component spectra for different rotations were observed, suggesting that the PMF solutions are robust and independent of rotation. The FPEAK=0 solution is used for further analysis. Regression analysis of Whistler Peak FTIR spectra was also performed to provide another means of estimating component contributions to ambient spectra. Spectra from combustion and three (non-burning) biogenic origins derived from PMF analysis of Whistler mid-valley spectra (R. E. Schwartz et al., 2010), and a BB spectrum from PMF decomposition of Scripps Pier spectra (Hawkins and Russell, 2010) were used as regressors (predictor variables). The explained variance (Eq. 1) is also used to assess the relative contributions of each component to ambient observations.

Potential Source Contribution Function (PSCF; Pekney et al., 2006) was also used to infer source regions from observed aerosol composition and concentrations, and air-mass backtrajectories obtained from the HYbrid Single Particle Lagrangian Integrated Trajectory Model (NOAA HYSPLIT; Draxler and Rolph, 2010). Six-day backtrajectories were calculated every two hours for the duration of the campaign at heights of 10, 100, and 500 m a.g.l. to consider the uncertainty of trajectories due to initial conditions. These trajectories were split according to pre-determined groups (by concentration order statistics or cluster analysis on explained variance of PMF factors).

3 Results and discussion

3.1 OM concentration and OFG composition

The OM was composed of alkane, carboxylic acid, ketone, organic hydroxyl, and amine groups and was highly variable throughout the project for all sample types as shown in Fig. 1. The OM project means and standard deviations for submicron samples,

ACPD
11, 2655–2696, 2011

total samples, and both submicron and total samples together, are 3.1±3.2 μg m^{-3}, 3.3±3.2 μg m^{-3}, and 3.2±3.3 μg m^{-3}, respectively. The mean OM of 4.1±3.5 μg m^{-3} during the second period (May to September) is significantly higher than the 0.6±0.3 μg m^{-3} mean concentration measured during the first month. This difference in the periods is emphasized by a comparison of the maximum concentrations of 1.2 μg m^{-3} and 13.6 μg m^{-3} during the first and second periods, respectively. The episodic variations in OM concentrations quantified by FTIR are also captured by co-located organic aerosol measurements from the ACSM, with a correlation coefficient of 0.88 and reduced major axis regression slope of 0.57 between the two methods. Applying a time-dependent collection-efficiency (0.49 on average) correction calculated from the ACSM ammonium to sulphate ratio (as described by Quinn et al., 2006), the correlation is 0.88 with major axis regression slope of 1.25.

The OFG composition as OM fraction is shown in Fig. 2. On average, organic hydroxyl, alkane, carboxylic acid, ketone, and amine groups represented 31%±11%, 34%±9%, 23%±6%, 6%±7%, and 6%±3% of OM, respectively. Organosulphate groups were above detection limit for only three samples collected during one sampling period (marked in Fig. 1) and represented 2 to 9% of OM when present. Two periods during which total OM was significantly larger than submicron OM are marked by a red bar in Fig. 1 and will be discussed further in Sect. 3.2. Acid group fraction and alkane group fraction are strongly correlated to each other (r=0.82) and moderately anti-correlated to organic hydroxyl group fraction (r=−0.74). Ketone groups were observed in the second time period only. In samples during the second period that had ketone groups above detection limit, ketone groups composed up to 27% of OM with an average of 14% of OM, indicating significant differences in environmental conditions favoring ketone group formation as observed at the Whistler Peak site. R. E. Schwartz et al. (2010) attributed the presence of non-acid carbonyl to biogenic (forest) emissions. In this study, the relative contribution of ketonic groups to the total OM mass was mildly to strongly correlated with BC number concentrations (r=0.79), total particle number concentrations (r=0.65), dust (r=0.56 to 0.75), and Br (r=0.75), more than

ACPD
11, 2655–2696, 2011

any other OFG. Ketone absorption was also observed in 18 out of 30 individual particles (Fig. 3) imaged by STXM-NEXAFS on 1 August and 21 August, and the overall absorption spectra and spherical shapes indicate that these particles are amorphous carbon tarballs produced during BB events (which exhibit ketone absorption) (Tivanski et al., 2007). The rest of the NEXAFS spectra did not have distinct signatures of functional group absorption (more observation of these nondescript particles are discussed by Takahama et al., 2007).

3.2 Size and diurnal comparison

Simultaneous total and submicron aerosol collection and analysis for OFG composition was used to calculate supermicron organic particles (supermicron=total minus submicron). The comparisons between the submicron and total OM and OFGs for both day and night are shown in Fig. 4. In all but a few samples, the total and submicron OM measurements compare very well and within the uncertainties of the measurements. The average total to submicron OM ratio is 0.99 with a correlation coefficient equal to 0.97. Total and submicron OM are indistinguishable during most samples, suggesting that little organic mass is present in supermicron particles. This is in contrast with trace metal concentrations analyzed by XRF on the same filters. For elements typically associated with dust emissions (Ti, Fe, Ca, K, Si, Al, Sr, Mn), their mass concentrations in submicron aerosol were 47–67% of that measured in the total samples; this fraction was consistent for each metal (correlation coefficient between these submicron and total aerosol concentrations were >0.95).

During two periods, 17 August to 21 August (night only) and 24 August to 31 August, a large difference between total and submicron OM measurements was observed, indicating OM was present in supermicron particles. A comparison between these submicron and supermicron OFG concentrations is shown in Fig. 5. In these four samples, the submicron OM concentrations are greater than the supermicron concentrations. Supermicron and submicron OFG composition is similar in all but the 17 August to 21 August night samples. A discussion of possible source influences during this period is discussed in Sect. 3.3.

ACPD
11, 2655–2696, 2011

Significant systematic differences between day and night samples were not observed in FTIR-quantified mass concentrations of OM and OFGs (Fig. 6). Diurnal variations are observed in concentrations of trace metals associated with dust emissions, however, with higher loadings observed during the day (night-time concentrations ranged between 43 and 86% of day-time concentrations and showed relatively consistent trends for each elements). The lack of large and systematic differences in OM suggests that on average, the measured aerosol originates from a regional rather than immediately local source, as temporal variation in source signatures is expected to be lost in aged air masses. Non-local aerosol sources are consistent with previous studies at the Whistler Peak location and are expected for this high-altitude, remote measurement site (Sun et al., 2009; Leaitch et al., 2009); this will again be discussed in Sect. 3.3.

3.3 Organic aerosol sources impacting the site

R. E. Schwartz et al. (2010) identified combustion and biogenic, or non-burning forest, sources during measurements in the spring at Whistler. Here we consider those sources plus the addition of BB which was prominent in the region for much of the summer. The British Columbia 2009 wildfire season was exceptionally severe in its length, number of fires, and area burned, and was accompanied by low precipitation. According to the British Columbia Wildfire Management branch, the 2009 fire season had one of the highest number of fires on record, with a total of 3040 fires (http://bcwildfire.ca/History/Summary.htm). During several time periods in the 2009 campaign, smoke was visible at the sampling site. Two separate fires occurred on Blackcomb mountain (less than 20 km from Whistler Peak) during 30 July to 8 August. As shown in Fig. 1, the largest OM concentrations measured by FTIR occurred for three samples collected between 28 July to 8 August, with reported concentrations of 10–14 $\mu g\,m^{-3}$. McKendry et al. (2010) also identified and studied another fire period between 29 August and 31 August using ceilometer and other measurements. We identify the contributions from these sources (combustion, biogenic, and BB) using

ACPD
11, 2655–2696, 2011

differences in perceived chemical and physical characteristics of the measured aerosol and components resolved by high time-resolution measurements, with additional insight gained from factor and regression analyses on FTIR spectra, and geo-spatial information regarding backtrajectories and fire locations.

Periods strongly influenced by burning and non-burning forest emissions are differentiated from those influenced heavily by anthropogenic combustion by examining the relative fraction of organic aerosol to organic and sulphate aerosol from the ACSM (Fig. 7a). During these forest-emission-dominated periods, this organic fraction is >70%. Episodes of BB are distinguished from non-burning periods by examining the count of local and regional fire hotspots (Fig. 8a, data provided by Natural Resources Canada (http://www.nrcan-rncan.gc.ca)) and increases in concentrations of mass fragments *m/z* 57, 60, and 73 (Fig. 7b; Schneider et al., 2006; Lee et al., 2010). The selection of these periods is confirmed by the rise in potassium to sulphate ratio (Fig. 8c) and calculated non-soil potassium concentrations (Fig. 8d), which are measured on a more coarse time resolution by filter-based methods. Lower values of cosine angle metric between ambient mass spectra and laboratory spectra of Shilling et al. (2009) are also observed during periods when the metrics for BB are low or absent. The mass spectra are more similar to the products of α-pinene ozonolysis, indicated by the lower values of this angle metric. The increasing ratio of *m/z* 44 to *m/z* 43 fragments indicates the presence of a more oxygenated organic aerosol (Ng et al., 2010) during BB periods compared to periods influenced by non-burning biogenic emissions. During these periods, BC number concentrations, coarse particle number concentrations, and mode of particle size distribution are also observed to increase, indicating a change in airmass. Though not specific to BB events, an increase in the particle mode diameter has been observed during such periods (e.g., Rissler et al., 2006).

Based on the above criteria, we identify periods or episodes described above in Figs. 7 and 8 as non-burning biogenic (green), BB (pink) and anthropogenic combustion (no colour). Their relationship to relative spatial distributions of backtrajectories and geographical features (cities, forests, and fire hotspots) are shown in Fig. 9 using

ACPD
11, 2655–2696, 2011

PSCF. The anthropogenic combustion periods are likely to be influenced by regional emissions from Northwest cities such as Vancouver and Seattle and pollutants from long-range transport of Asian emissions (Fig. 9a), consistent with measurements of sulphate at Whistler Peak by Sun et al. (2009). Meteorological trajectories extending back 5 days indicate another set of trajectories with possible origins from Asia, outside of the domain of PSCF analysis. In agreement with the fire count time series shown previously, PSCF maps indicate collectively lower fire counts during non-burning biogenic source periods than biomass-burning periods, and wind trajectories arrive to Whistler Peak from the north over forested regions (Fig. 9b). During BB episodes, airmasses appear to arrive primarily from northeast of the site after passing near or over hotspots during fire periods (Fig. 9c), concurrent with smoke and reduced visibility often reported at the peak site. Fig. 9 supports the attribution of periods to emission sources.

To interpret the influence of source on measured OFGs, a hierarchical clustering algorithm (Ward, 1963) is applied to the set of submicron aerosol spectra (Fig. 10) after normalizing by their respective dot products (Murphy et al., 2003). The result is a set of several categories containing spectra with similar features, and the membership of each filter to these categories in time is illustrated in the lower panel of Fig. 10. We interpret the features present in the spectra in the context of FTIR PMF factors derived from previous campaigns (R. E. Schwartz et al., 2010; Hawkins and Russell, 2010), and assess relative contributions of these components to each cluster by regression analysis. The results from the regression analysis may be considered qualitative, as they are dependent upon the assumptions regarding (1) components present in each sample and (2) absorption profiles of the components. In addition, some degree of collinearity is present in the spectra profiles combined from the previous campaigns. For instance, the correlation between spectral profiles of the Combustion and Biogenic Part 1 from Whistler mid-valley, and Biogenic Part 3 from Whistler mid-valley and the Scripps Pier BB factor components are both 0.82, leading to an inflated variance in contribution estimates. This effect may lead to higher uncertainty in apportioned values between the

ACPD
11, 2655–2696, 2011

combustion and forest component, and between the forest and BB components. However, these results provide first-order insights into the relative contribution of different source components to each spectra type.

Spectra in category (a) are suggested to have origins in fossil-fuel anthropogenic combustion. Aerosols having this spectra are accompanied by sulphur concentrations twice as high on average (uncorrected value of 0.8 $\mu g\,m^{-3}$) as during other periods, and FTIR spectral profiles resemble combustion factors identified at the Whistler mid-mountain site and other field campaigns (Russell et al., 2009; Liu et al., 2009; Hawkins and Russell, 2010). This spectra type or component has the characteristic ammonium absorbance that is observed for the combustion factors identified by PMF on FTIR spectra, and its organic fraction contains large fractions of alkane and acid (39 and 26%, respectively, on average), with little contribution from ketonic groups. This category of aerosols appear to contain more organic hydroxyl than combustion factors derived from PMF (hydroxyl mass fraction is on average 30%, contrasted with 17% at Whistler mid-valley, R. E. Schwartz et al., 2010). This suggests a mix of combustion with biogenic (R. E. Schwartz et al., 2010) or marine sources (**?**), as forests around Whistler or the Pacific Ocean may contribute to the organic aerosol transported to the site from combustion sources. Regression analysis using combustion, forest, and BB sources supports this interpretation (Fig. 10a′), indicating the largest contributions from anthropogenic combustion (70% on average), with smaller contributions (24% on average) from forest components. As the Whistler Peak is surrounded by forest sources, it is not surprising to find forest contributions to all samples. Aerosols with spectra belonging in this cluster were collected during periods not designated as non-burning biogenic or burning periods, suggesting that indeed the primary source of influence is likely to be anthropogenic combustion.

Spectra in category (c) resembles the combined (non-burning) biogenic factor from the 2008 campaign at Whistler mid-valley (R. E. Schwartz et al., 2010; Fig. 11b). This factor is not dominated by any one functional group, but is distributed as 34% alkane, 24% acid, 20% hydroxyl, and 14% carbonyl on average. While aerosols with type (c)

ACPD
11, 2655–2696, 2011

spectra were collected during several different periods, two spectra in this category were the only ones observed largely within the bounds of the non-burning biogenic periods (between 20 July and 28 July, Fig. 10f′). Regression analysis also supports this interpretation, with strongest contributions from non-burning forest sources (66%; Fig. 10c′).

Spectra in category (e) strongly resemble the BB factor from Scripps Pier measurements (Hawkins and Russell, 2010) made in San Diego, CA, and are characterized by high carbonyl and amine absorption (on average, 26 and 19% of OM, respectively), very little organic hydroxyl (6% on average), and a pair of sharp peaks at 2920 cm^{-1} and 2850 cm^{-1}. These spectra were observed sometime during the evenings of 17 August to 21 August and 31 August to 3 September, which were periods pre-determined to be influenced by fire emissions (Fig. 10f′). This pair of sharp peaks has been observed and briefly described by Hawkins and Russell (2010). The authors observed this same spectral feature in a subset of samples collected at the Scripps Pier during summer 2008, and in their identified BB PMF factor (Fig. 11e). The sharpness of the peaks, which are located at the sp^3 C–H stretching absorption from methylene groups, is suggested to originate from repeating methylene units in long-chain plant cuticle wax detritus (Hawkins and Russell, 2010). Hawkins and Russell (2010) report several observations in which these compounds were lofted in large wildfires (Simoneit, 1985; Fang et al., 1999; Simoneit et al., 2004; Medeiros et al., 2006), but presence of these peaks in aerosol spectra from Whistler mid-valley in 2008 (as shown in a biogenic factor component in Fig. 11d) – where contributions from wildfire burning were estimated to be minimal – suggests that similar compounds may be emitted from non-burning forest sources. Their co-occurence with dust (R. E. Schwartz et al., 2010) suggests the lofting of detritus even in the absence of fires. Regression analysis also supports this interpretation, with BB contributions explaining 60% of the variation, with 20% contribution from forest components (Fig. 10e′).

Spectra in categories (b) and (d) (Fig. 10b and d, respectively) appear to contain a mix of sources, more than the other three categories, and their occurrence in time

ACPD
11, 2655–2696, 2011

indicates that their collection times straddle more than one source period (Fig. 10f′). Spectra type (b) appears to have a peak at 3100 cm^{-1} [as does type (a)], suggesting the presence of ammonium, but also contains methylene peaks, hydroxyl, and carbonyl; this is possibly a mix of combustion, non-burning biogenic, and BB aerosol. Spectra type (d) shows a strong hydroxyl signature with methylene peaks and carbonyl absorption, and occurs primarily during non-burning biogenic and BB periods. Similarity to a combined forest (burning and non-burning) PMF factor (2-factor solution, discussed below) for this spectra set, suggests that this is a plausible interpretation. Given the remote location of the Whistler Peak sampling site and three to five-day collection times, the occurrence of such a mixture would not be surprising. Relative contributions in each mixture is supported by regression analysis; with variations explained by anthropogenic combustion, non-burning forest, and BB with on the order of 28, 53, and 13% for spectra category (b), and 9, 60, and 23% for category (d), respectively (Fig. 10b′ and d′).

PMF analysis was also applied to the FTIR spectra for submicron aerosols to determine if the mixed aerosol types can be resolved into constituent profiles and contributions. In two- to six-factor PMF decompositions, one factor (Fig. 11a) sharing spectroscopic characteristics of the combustion cluster (Fig. 10a) consistently appears with little change in profile or strength among rotations and number of factors, while the remaining variance is divided among the other factor(s). The three-factor solution will be discussed primarily as its profiles can be interpreted fairly clearly from comparison with PMF factors from past projects. This solution explained 90% of the variance in the spectra, on average. In this solution, one of the two remaining factors closely resembles the BB component spectra reported by Hawkins and Russell (2010), as seen in Fig. 11e, and for this reason it is referred to as Factor BB. The Factor BB spectra contains the sharp methylene double peaks noted earlier, and relatively high absorbance by ketone groups. A large fractional contribution of ketone has not been observed in combustion or marine FTIR PMF components, but has been observed in both BB and biogenic sources (Hawkins and Russell, 2010; R. E. Schwartz et al., 2010; Bahadur

ACPD
11, 2655–2696, 2011

et al., 2010). Hawkins and Russell (2010) also observed a significant fraction of ketone in their BB fraction at the Scripps Pier. The ketone fraction of Factor BB is similar to that reported by Hawkins and Russell (2010) (25%). Factor BB is correlated to Br (r=0.67) and non-soil K (r=0.69), which are considered to be tracers for BB (Andreae et al., 1996 and Gilardoni et al., 2009, respectively). The spectral profile of Factor BB also resembles the spectra cluster shown in Fig. 10e (corresponding to sampling periods 17 August to 21 August and 31 August to 3 September). The number of samples in this category is small, but appears to be an "edge" case in the search space of PMF. Edge cases represent events in which one or few sources dominate mixture proportions, providing better constraints on component identities (Henry, 2003). The spectral profile of the remaining factor resembles non-burning forest emissions and is referred to as Factor Bio. The Factor Bio spectrum resembles the high-hydroxyl "Biogenic Part 1" identified from the mid-mountain Whistler measurements of R. E. Schwartz et al. (2010) (Fig. 11c). Biogenic Part 1 was correlated to monoterpenes and dust. Factor Bio has a ketone contribution unlike Biogenic Part 1, but similar to the combined Whistler 2008 biogenic factor (Fig. 11b). The presence of ketone is supportive of BVOC oxidation, as suggested by laboratory chamber studies of monoterpene and isoprene oxidation products (Table 2 of R. E. Schwartz et al., 2010) and measurements of ambient aerosol influenced by forest sources (Bahadur et al., 2010). Ketonic carbonyl was not observed in the total, continuous samples during non-burning forest aerosol (Fig. 2), while it was observed in the submicron and total samples when for day or night-only samples. The carbonyl absorption for the total, continuous periods were not below detection limit, but (unambiguously) apportioned to carboxylic acid rather than ketonic carbonyl according to the algorithm described in Russell et al. (2009). The methylene peaks also appear in Factor Bio, which is a reasonable outcome if long-chain plant waxes are lofted by the wind from non-burning forest sources.

While the combustion factor is highly prominent in the low OM period in March and April, the two forest (burning and non-burning) sources are the main contributors to the high OM during May to September (Fig. 12a,b), a period characterized by higher

ACPD
11, 2655–2696, 2011

temperatures and numerous sporadic fires. The contribution of Factor Bio to the first period when there were no fires is higher relative to Factor BB. It is worth noting, however, that Factor BB and Factor Bio have an apparent correlation coefficient of 0.88. As discussed previously, multi-collinearity is a well-known issue in regression problems, and its presence indicates that the variance in estimated strengths of our components are likely to be inflated. Observations suggest that this is the case for Factor Bio and Factor BB. During the large local fire period of 30 July to 8 August the relative contribution of Factor Bio increases rather than Factor BB. Factor BB, in small contributions, is observed during time periods of no to little wildfires such as the first period and early July. For these periods, it is likely that the magnitude of component strengths cannot be differentiated from each other in the former case, or from zero in the latter example. Also, in the case of PMF analysis where component strengths and profiles are both estimated from the data, it is possible that errors in the estimated coefficients (strengths) may also lead to errors in the factor profiles. The close resemblance of factor profiles for the Whistler Peak site to profiles derived for other campaigns and independently attributed to probable sources (e.g., Hawkins and Russell, 2010; R. E. Schwartz et al., 2010) suggests that the error in overall shape of our profiles is small.

Exploring other possible solutions, we find that the four-factor solution retains the combustion factor but further splits Factor BB into component profiles previously unobserved in ambient and laboratory spectra. As Ulbrich et al. (2009) point out, components can be arbitrarily "split" into artificial factors once the prescribed number of factors exceeds the number of resolvable components, which may be a possible interpretation in this case. The two-factor solution contains the combustion factor and a factor combining the features of the burning and non-burning forest factors (methylene peaks and high carbonyl absorbance) as shown in Fig. 11d. This solution explained 80% of the variation on average, but the explained variation was approximately 30% for type (e) samples (BB) and was as low as 62–64% for some samples in cluster (c) (non-burning biogenic), suggesting that this forest factor does not represent the extreme cases of

ACPD
11, 2655–2696, 2011

burning and non-burning products well. The similarity of the two combustion factors both in composition and in temporal contribution to OM over the whole campaign as shown in Fig. 12 is noteworthy. This robustness in the combustion factor profile and strength suggests that combustion is a chemically consistent source of organic aerosol to Whistler Peak.

The spectral profiles derived from PMF correspond to the average profiles of components contributing to Eulerian measurements at a fixed location (e.g., Whistler Peak). When relating possibly non-conservative components to source profiles, we implicitly invoke the assumption of quasi-stationarity (Zhou et al., 2005). If chemical transformations are occurring during transport (and are reflected in the observed spectra at the site), the transformations must be relatively consistent for each of the PMF components such that each component represents the contributions from the primary emission signature and a (semi-)constant transformation term. When rates of transport dominate over transformation mechanisms across arbitrary distances for aerosols with regional sources, observations of homogeneous composition over space and time can be observed. The similarity of the combustion and forest PMF factors from this study to those derived for the Whistler mid-valley campaign suggests that the aerosols are probably non-local to either of these locations, and may be the product of common sources and chemical transformations. The absence of significant day-night differences observed in this study (Fig. 6) is consistent with the observation that the OM was not dominated by local-scale sources (e.g., daytime photochemistry), and is also consistent with a long-range transported combustion source or forest burning courses (either local or regional). Even a non-burning forest source such as BVOC oxidation may not exhibit a diurnal signal in the OM as the daytime increments from oxidants, potentially increased BVOC, and transport time from valley to the Peak may not permit sufficient distinction relative to the existing aerosol, particularly with 12-h integrated filters. The spectral similarity in the BB factor at Whistler Peak and Scripps Pier is surprising, given the possible differences in atmospheric processing that may occur during transport from fire locations in Western Canada or Northern California to their respective

ACPD
11, 2655–2696, 2011

measurement sites. This resemblance may reflect the similarity in chemical composition of organic aerosols emitted from BB sources, but may also reflect the similarity in the chemistry occurring in BB plumes (e.g., VOCs released during burning might be reduced to similar dominant compounds).

The 21 August to 24 August three-day sample was the only period for which organosulphate groups were above detection limit. This period also corresponds to the highest sulphate concentrations measured by ACSM (6-h averaged concentrations (uncorrected for collection efficiency) peaking at 6 $\mu g\,m^{-3}$). The combination of organosulphate groups and supermicron organic particles suggests that air masses sampled from 17 August to 31 August may have been influenced by different sources than those controlling the particle composition during most of the project. On 17 August 2009 the Koryaksky Volcano in Kamchatka, Russia erupted sending emissions to at least a height of 4000 m a.s.l. and causing an air traffic advisory to be issued. Air back-trajectories reach to this general area (Fig. 13), offering the possibility that this increase in sulphur, primarily sulphuric acid, was the result of the transport and oxidation of SO_2 from this eruption. However, the general feature of lower organic and higher sulphate mass concentrations is also consistent with the Trans-Pacific transport of Asia pollution to this site (e.g., Leaitch et al., 2009). In either case, a long distance source is a likely explanation.

3.4 Mid-mountain and peak comparison

Through a comparison between the Whistler mid-valley 2008 (1020 m a.s.l.) and a period of Whistler Peak 2009 measurements the impact of terrain on measured OFG concentrations and on aerosol influences can be examined. Whistler 2008 submicron ~12 h measurements were collected for a month from 16 May to 16 June 2008 (Schwartz et al., 2010). The 2008 submicron OM at the valley site ranged from less than 0.5 to 3.1 $\mu g\,m^{-3}$, with a project mean and standard deviation of 1.3±1.0 $\mu g\,m^{-3}$. The 2009 measurements from 23 May to 17 June (the most comparable time period) ranged from less than 1.3 to 5.1 $\mu g\,m^{-3}$, with a project mean and standard deviation

ACPD
11, 2655–2696, 2011

of 3.6±1.6 µg m^{-3}. The 2009 peak OM concentrations were significantly higher than those measured at the mid-valley site in 2008. The OFG composition for 2008 and the 2009 period were respectively 34% and 23% organic hydroxyl, 33% and 37% alkane, 23% and 26% carboxylic acid, 6% and 9% ketone, and 5% and 5% amine groups. One notable difference between the sites is that trees surround the 2008 mid-mountain site, while the Whistler Peak site is above the tree line. In addition to the elevation difference, differences between the 2008 and 2009 measurements may be a result of the early 2009 fire season, with influences from BB aerosol in early June of 2009 skewing the comparison. In contrast to 2009, the 2008 fire season started slowly due to cool spring temperatures, and R. E. Schwartz et al. (2010) did not observe a BB influence for the Whistler 2008 study.

4 Conclusions

Three-day ambient OM concentrations measured at Whistler Peak during spring and summer 2009 varied from 0.06 to 13.6 µg m^{-3} with a project mean and standard deviation of 3.2±3.3 µg m^{-3}. Significant systematic trends were not observed in FTIR measurements between day- and night-time samples. Submicron and total OFG mass concentrations were indistinguishable, with the exception of a few periods. The OM concentrations, which reached 1.2 µg m^{-3} during the first period of sampling from March to April, were consistently lower than the concentrations from May to September. Ketone groups were not detected in the first period but contributed up to 27% of the average organic aerosol composition in the second period.

The OM concentrations measured during spring 2008 in the Whistler valley, at a site over 1 km lower than the peak location, were lower than the concentrations observed during the corresponding time period at the peak in 2009. The average OFG composition of the submicron aerosol was in general similar between the two sites. Most notably, 11% by mass less organic hydroxyl groups were observed in the peak measurements. However, this comparison of OM is influenced by the early start of the

ACPD
11, 2655–2696, 2011

2009 fire season. The 2009 forest fire season in British Columbia set a record for most recorded fires while the total area burned was well above average. The fire season was also longer than usual, with notable fires in September and multiple fires burning as early as May due to abnormally high temperatures and low precipitation.

From an analysis of aerosol measurements and airmass backtrajectories, the sampling campaign was divided into periods primarily influenced by anthropogenic combustion, non-burning forest emissions, and biomass burning sources. FTIR aerosol spectra resembling the anthropogenic combustion PMF factor from the Whistler mid-valley campaign (2008) were observed during the combustion periods. These spectra have a characteristic ammonium absorbance (often associated with sulphate) and are dominated by alkane functional groups (39% on average) in the organic aerosol fraction. Spectra of aerosols collected during a few biomass burning periods resembled the biomass burning component from the Scripps Pier campaign (2008) in San Diego, CA. This spectra type contained sharp methylene peaks attributed to plant waxes, and a large contribution of non-acid carbonyl (26% on average) to the organic aerosol mass. Spectra resembling non-burning biogenic forest component from the Whistler mid-valley campaign were also observed during periods determined to be dominated by non-burning biogenic sources. The remaining FTIR spectra appeared to contain a mixture or aerosols from these three sources, which is a plausible outcome due to the remoteness of the sampling location and three to five-day sampling intervals. PMF decomposition of this spectra set revealed components (combustion, non-burning biogenic, and burning) similar or nearly identical to factors found in previous campaigns.

Acknowledgements. The authors would like to thank Whistler Blackcomb, Juniper Buller, Anton Horvath, and John Shilling for providing the spectra, and Natural Resources Canada (NRCan) and John Little for the fire hotspot data.

ACPD
11, 2655–2696, 2011

References

Allan, J. D., Delia, A. E., Coe, H., Bower, K. N., Alfarra, M. R., Jimenez, J. L., Middlebrook, A. M., Drewnick, F., Onasch, T. B., Canagaratna, M. R., Jayne, J. T., and Worsnop, D. R.: A generalised method for the extraction of chemically resolved mass spectra from aerodyne aerosol mass spectrometer data, J. Aerosol Sci., 35, 909–922, 2004. 2660

Andreae, M. O., Atlas, E., Harris, G. W., Helas, G., deKock, A., Koppmann, R., Maenhaut, W., Mano, S., Pollock, W. H., Rudolph, J., Scharffe, D., Schebeske, G., and Welling, M.: Methyl halide emissions from savanna fires in Southern Africa, J. Geophys. Res.-Atmos., 101, 23603–23613, 1996. 2672

Bahadur, R., Uplinger, T., Russell, L. M., Sive, B. C., Cliff, S. S., Millet, D. B., Goldstein, A., and Bates, T. S.: Phenol Groups in Northeastern US Submicrometer Aerosol Particles Produced from Seawater Sources, Environ. Sci. Technol., 44, 2542–2548, 2010. 2671, 2672

Bond, T. C., Streets, D. G., Yarber, K. R., Nelson, S. M., Woo, W. J.-H., and Klimont, Z.: A technology-based global inventory of black and organic carbon emissions from combustion, J. Geophys. Res., 109(D14), D14203, doi:10.1029/2003JD003697, 2004. 2656

Bowman, D. M. J. S., Balch, J. K., Artaxo, P., Bond, W. J., Carlson, J. M., Cochrane, M. A., D'Antonio, C. M., DeFries, R. S., Doyle, J. C., Harrison, S. P., Johnston, F. H., Keeley, J. E., Krawchuk, M. A., Kull, C. A., Marston, J. B., Moritz, M. A., Prentice, I. C., Roos, C. I., Scott, A. C., Swetnam, T. W., van der Werf, G. R., and Pyne, S. J.: Fire in the Earth system, Science, 324, 481–484, 2009. 2657

Canagaratna, M. R., Jayne, J. T., Jimenez, J. L., Allan, J. D., Alfarra, M. R., Zhang, Q., Onasch, T. B., Drewnick, F., Coe, H., Middlebrook, A., Delia, A., Williams, L. R., Trimborn, A. M., Northway, M. J., DeCarlo, P. F., Kolb, C. E., Davidovits, P., and Worsnop, D. R.: Chemical and microphysical characterization of ambient aerosols with the aerodyne aerosol mass spectrometer, Mass Spectrom. Rev., 26, 185–222, 2007. 2660

Cross, E., Onasch, T., Ahern, A., Wrobel, W., Slowik, J., Olfert, J., Lack, D., Massoli, P., Cappa, C., Schwarz, J., 2661
Spackman, J. R., Fahey, D. W., Sedlacek, A., Trimborn, A., Jayne, J. T., Freedman, A., Williams, L. R., Ng, N. L., Mazzoleni, C., Dubey, M., Brem, B., Kok, G., Subramanian, R., Freitag, S., Clarke, A., Thornhill, D., Marr, L. C., Kolb, C. E., Worsnop, D. R., and Davidovits, P.: Soot Particle Studies – Instrument Inter-Comparison – Project Overview, Aerosol Sci. Tech., 44, 592–611, 2010.

ACPD
11, 2655–2696, 2011

Draxler, R. and Rolph, G.: HYSPLIT (HYbrid Single-Particle Lagrangian Integrated Trajectory) Model access via NOAA ARL READY Website (http://ready.arl.noaa.gov/HYSPLIT.php), 2010. 2663

Fang, M., Zheng, M., Wang, F., To, K., Jaafar, A., and Tong, S.: The solvent-extractable organic compounds in the Indonesia biomass burning aerosols-characterization studies, Atmos. Environ., 33, 783–795, 1999. 2670

Gilardoni, S., Liu, S., Takahama, S., Russell, L. M., Allan, J. D., Steinbrecher, R., Jimenez, J. L., De Carlo, P. F., Dunlea, E. J., and Baumgardner, D.: Characterization of organic ambient aerosol during MIRAGE 2006 on three platforms, Atmos. Chem. Phys., 9, 5417–5432, doi:10.5194/acp-9-5417-2009, 2009. 2672, 2691

Hallquist, M., Wenger, J. C., Baltensperger, U., Rudich, Y., Simpson, D., Claeys, M., Dommen, J., Donahue, N. M., George, C., Goldstein, A. H., Hamilton, J. F., Herrmann, H., Hoffmann, T., Iinuma, Y., Jang, M., Jenkin, M. E., Jimenez, J. L., Kiendler-Scharr, A., Maenhaut, W., McFiggans, G., Mentel, Th. F., Monod, A., Prévôt, A. S. H., Seinfeld, J. H., Surratt, J. D., Szmigielski, R., and Wildt, J.: The formation, properties and impact of secondary organic aerosol: current and emerging issues, Atmos. Chem. Phys., 9, 5155–5236, doi:10.5194/acp-9-5155-2009, 2009. 2656, 2657

Hawkins, L. N. and Russell, L. M.: Oxidation of ketone groups in transported biomass burning aerosol from the 2008 Northern California Lightning Series fires, Atmos. Environ., 44, 4142–4154, 2010. 2662, 2663, 2668, 2669, 2670, 2671, 2672, 2673, 2694

Heald, C. L., Jacob, D. J., Park, R. J., Russell, L. M., Huebert, B. J., Seinfeld, J. H., Liao, H., and Weber, R. J.: A large organic aerosol source in the free troposphere missing from current models, Geophys. Res. Lett., 32, L18809, doi:10.1029/2005GL023831, 2005. 2657

Heald, C. L., Jacob, D. J., Turquety, S., Hudman, R. C., Weber, R. J., Sullivan, A. P., Peltier, R. E., Atlas, E. L., de Gouw, J. A., Warneke, C., Holloway, J. S., Neuman, J. A., Flocke, F. M., and Seinfeld, J. H.: Concentrations and sources of organic carbon aerosols in the free troposphere over North America, J. Geophys. Res.-Atmos., 111, D23S47, doi:10.1029/2006JD007705, 2006. 2657

Henry, R. C.: Multivariate receptor modeling by *N*-dimensional edge detection, Chemometr. Intell. Lab., 65, 179–189, 2003. 2672

Intergovernmental Panel on Climate Change: IPCC: Climate Change 2007: The Physical Science Basis, Contribution of Working Group I to the Fourth Assessment Report of the Intergovernmental Panel on Climate Change, Tech. rep., 2007. 2657

ACPD

11, 2655–2696, 2011

Jayne, J. T., Leard, D. C., Zhang, X. F., Davidovits, P., Smith, K. A., Kolb, C. E., and Worsnop, D. R.: Development of an aerosol mass spectrometer for size and composition analysis of submicron particles, Aerosol Sci. Tech., 33, 49–70, 2000. 2660

Kulmala, M., Suni, T., Lehtinen, K. E. J., Dal Maso, M., Boy, M., Reissell, A., Rannik, Ü., Aalto, P., Keronen, P., Hakola, H., Bäck, J., Hoffmann, T., Vesala, T., and Hari, P.: A new feedback mechanism linking forests, aerosols, and climate, Atmos. Chem. Phys., 4, 557–562, doi:10.5194/acp-4-557-2004, 2004. 2657

Leaitch, W. R., Macdonald, A. M., Anlauf, K. G., Liu, P. S. K., Toom-Sauntry, D., Li, S.-M., Liggio, J., Hayden, K., Wasey, M. A., Russell, L. M., Takahama, S., Liu, S., van Donkelaar, A., Duck, T., Martin, R. V., Zhang, Q., Sun, Y., McKendry, I., Shantz, N. C., and Cubison, M.: Evidence for Asian dust effects from aerosol plume measurements during INTEX-B 2006 near Whistler, BC, Atmos. Chem. Phys., 9, 3523–3546, doi:10.5194/acp-9-3523-2009, 2009. 2666, 2675

Lee, T., Sullivan, A. P., Mack, L., Jimenez, J. L., Kreidenweis, S. M., Onasch, T. B., Worsnop, D. R., Malm, W., Wold, C. E., Hao, W. M., and Collett, J. L.: Chemical Smoke Marker Emissions During Flaming and Smoldering Phases of Laboratory Open Burning of Wildland Fuels, Aerosol Sci. Tech., 44, I–V, 2010. 2667

Liu, B. Y. H., Romay, F. J., Dick, W. D., Woo, K. S., and Chiruta, M.: A Wide-Range Particle Spectrometer for Aerosol Measurement from 0.010 µm to 10 µm, Aerosol Air Qual. Res., 10, 125–139, 2010. 2659

Liu, S., Takahama, S., Russell, L. M., Gilardoni, S., and Baumgardner, D.: Oxygenated organic functional groups and their sources in single and submicron organic particles in MILAGRO 2006 campaign, Atmos. Chem. Phys., 9, 6849–6863, doi:10.5194/acp-9-6849-2009, 2009. 2669

Maria, S. F., Russell, L. M., Turpin, B. J., Porcja, R. J., Campos, T. L., Weber, R. J., and Huebert, B. J.: Source signatures of carbon monoxide and organic functional groups in Asian Pacific Regional Aerosol Characterization Experiment (ACE-Asia) submicron aerosol types, J. Geophys. Res.-Atmos., 108(D23), 8637, doi:10.1029/2003JD003703, 2003. 2659

McKendry, I. G., Gallagher, J., Campuzano Jost, P., Bertram, A., Strawbridge, K., Leaitch, R., and Macdonald, A. M.: Ground-based remote sensing of an elevated forest fire aerosol layer at Whistler, BC: implications for interpretation of mountaintop chemistry, Atmos. Chem. Phys., 10, 11921–11930, doi:10.5194/acp-10-11921-2010, 2010. 2666

Medeiros, P. M., Conte, M. H., Weber, J. C., and Simoneit, B. R. T.: Sugars as source indicators

ACPD

11, 2655–2696, 2011

of biogenic organic carbon in aerosols collected above the Howland Experimental Forest, Maine, Atmos. Environ., 40, 1694–1705, 2006. 2670

Murphy, D. M., Middlebrook, A. M., and Warshawsky, M.: Cluster analysis of data from the Particle Analysis by Laser Mass Spectrometry (PALMS) instrument, Aerosol Sci. Tech., 37, 382–391, 2003. 2668

Ng, N. L., Canagaratna, M. R., Zhang, Q., Jimenez, J. L., Tian, J., Ulbrich, I. M., Kroll, J. H., Docherty, K. S., Chhabra, P. S., Bahreini, R., Murphy, S. M., Seinfeld, J. H., Hildebrandt, L., Donahue, N. M., DeCarlo, P. F., Lanz, V. A., Prévôt, A. S. H., Dinar, E., Rudich, Y., and Worsnop, D. R.: Organic aerosol components observed in Northern Hemispheric datasets from Aerosol Mass Spectrometry, Atmos. Chem. Phys., 10, 4625–4641, doi:10.5194/acp-10-4625-2010, 2010. 2667

Ng, N. L., Herndon, S. C., Trimborn, A., Canagaratna, M. R., Croteau, P., Onasch, T. B., Sueper, D., Worsnop, D. R., Zhang, Q., Sun, Y. L., and Jayne, J. T.: An Aerosol Chemical Speciation Monitor (ACSM) for routine monitoring of the composition and mass concentrations of ambient aerosol, Aerosol Sci. Technol., in press, 2011. 2660

Paatero, P.: Users Guide for Positive Matrix Factorization programs PMF2 and PMF3, Part 2: reference, University of Helsinki, Department of Physics, 2007. 2662

Paatero, P. and Tapper, U.: Positive matrix factorization – a nonnegative factor model with optimal utilization of error-estimates of data values, Environmetrics, 5, 111–126, 1994. 2662

Pekney, N. J., Davidson, C. I., Zhou, L. M., and Hopke, P. K.: Application of PSCF and CPF to PMF-modeled sources of $PM_{2.5}$ in Pittsburgh, Aerosol Sci. Tech., 40, 952–961, 2006. 2663

Penner, J. E., Zhang, S. Y., and Chuang, C. C.: Soot and smoke aerosol may not warm climate, J. Geophys. Res.-Atmos., 108(D21), 4657, doi:10.1029/2003JD003409, 2003. 2657

Quinn, P. K., Bates, T. S., Coffman, D., Onasch, T. B., Worsnop, D., Baynard, T., de Gouw, J. A., Goldan, P. D., Kuster, W. C., Williams, E., Roberts, J. M., Lerner, B., Stohl, A., Pettersson, A., and Lovejoy, E. R.: Impacts of sources and aging on submicrometer aerosol properties in the marine boundary layer across the Gulf of Maine, J. Geophys. Res.-Atmos., 111, D23S36, doi:10.1029/2006JD007582, 2006. 2664

Rissler, J., Vestin, A., Swietlicki, E., Fisch, G., Zhou, J., Artaxo, P., and Andreae, M. O.: Size distribution and hygroscopic properties of aerosol particles from dry-season biomass burning in Amazonia, Atmos. Chem. Phys., 6, 471–491, doi:10.5194/acp-6-471-2006, 2006. 2667

Russell, L. M., Takahama, S., Liu, S., Hawkins, L. N., Covert, D. S., Quinn, P. K., and Bates, T. S.: Oxygenated fraction and mass of organic aerosol from direct emission and

ACPD
11, 2655–2696, 2011

atmospheric processing measured on the R/V Ronald Brown during TEXAQS/GoMACCS 2006, J. Geophys. Res.-Atmos., 114, D00F05, doi:10.1029/2008JD011275, 2009. 2658, 2659, 2662, 2669, 2672

Schneider, J., Weimer, S., Drewnick, F., Borrmann, S., Helas, G., Gwaze, P., Schmid, O., Andreae, M., and Kirchner, U.: Mass spectrometric analysis and aerodynamic properties of various types of combustion-related aerosol particles, Int. J. Mass Spectrom., 258, 37–49, 2006. 2667

Schwartz, R. E., Russell, L. M., Sjostedt, S. J., Vlasenko, A., Slowik, J. G., Abbatt, J. P. D., Macdonald, A. M., Li, S. M., Liggio, J., Toom-Sauntry, D., and Leaitch, W. R.: Biogenic oxidized organic functional groups in aerosol particles from a mountain forest site and their similarities to laboratory chamber products, Atmos. Chem. Phys., 10, 5075–5088, doi:10.5194/acp-10-5075-2010, 2010. 2662, 2663, 2664, 2666, 2668, 2669, 2670, 2671, 2672, 2673, 2676, 2694

Schwarz, J. P., Spackman, J. R., Gao, R. S., Perring, A. E., Cross, E., Onasch, T. B., Ahern, A., Wrobel, W., Davidovits, P., Olfert, J., Dubey, M. K., Mazzoleni, C., and Fahey, D. W.: The Detection Efficiency of the Single Particle Soot Photometer, Aerosol Sci. Tech., 44, 612–628, 2010.

Seinfeld, J. H. and Pandis, S. N.: Atmospheric Chemistry and Physics, second edn., John Wiley & Sons, New York, 2006. 2656

Shilling, J. E., Chen, Q., King, S. M., Rosenoern, T., Kroll, J. H., Worsnop, D. R., DeCarlo, P. F., Aiken, A. C., Sueper, D., Jimenez, J. L., and Martin, S. T.: Loading-dependent elemental composition of -pinene SOA particles, Atmos. Chem. Phys., 9, 771–782, doi:10.5194/acp-9-771-2009, 2009. 2662, 2667, 2690

Simoneit, B. R. T.: Application of molecular marker analysis to vehicular exhaust for source reconciliations, Int. J. Environ. An. Ch., 22, 203–233, 1985. 2670

Simoneit, B. R. T., Kobayashi, M., Mochida, M., Kawamura, K., and Huebert, B. J.: Aerosol particles collected on aircraft flights over the Northwestern Pacific region during the ACE-Asia campaign: Composition and major sources of the organic compounds, J. Geophys. Res.-Atmos., 109, D19S10, doi:10.1029/2004JD004598, 2004. 2670

Stöhr, J.: NEXAFS Spectroscopy, Springer-Verlag, Berlin, 1992. 2659

Subramanian, R., Kok, G. L., Baumgardner, D., Clarke, A., Shinozuka, Y., Campos, T. L., Heizer, C. G., Stephens, B. B., de Foy, B., Voss, P. B., and Zaveri, R. A.: Black carbon over Mexico: the effect of atmospheric transport on mixing state, mass absorption cross-section,

ACPD
11, 2655–2696, 2011

and BC/CO ratios, Atmos. Chem. Phys., 10, 219–237, doi:10.5194/acp-10-219-2010, 2010. 2661

Sun, Y., Zhang, Q., Macdonald, A. M., Hayden, K., Li, S. M., Liggio, J., Liu, P. S. K., Anlauf, K. G., Leaitch, W. R., Steffen, A., Cubison, M., Worsnop, D. R., van Donkelaar, A., and Martin, R. V.: Size-resolved aerosol chemistry on Whistler Mountain, Canada with a high-resolution aerosol mass spectrometer during INTEX-B, Atmos. Chem. Phys., 9, 3095–3111, doi:10.5194/acp-9-3095-2009, 2009. 2666

Takahama, S., Gilardoni, S., Russell, L. M., and Kilcoyne, A. L. D.: Classification of multiple types of organic carbon composition in atmospheric particles by scanning transmission X-ray microscopy analysis, Atmos. Environ., 41, 9435–9451, 2007. 2665

Takahama, S., Liu, S., and Russell, L. M.: Coatings and clusters of carboxylic acids in carbon-containing atmospheric particles from spectromicroscopy and their implications for cloud-nucleating and optical properties, J. Geophys. Res.-Atmos., 115, D01202, doi:10.1029/2009JD012622, 2010. 2659

Tivanski, A. V., Hopkins, R. J., Tyliszczak, T., and Gilles, M. K.: Oxygenated interface on biomass burn tar balls determined by single particle scanning transmission X-ray microscopy, J. Phys. Chem. A, 111, 5448–5458, 2007. 2665

Ulbrich, I. M., Canagaratna, M. R., Zhang, Q., Worsnop, D. R., and Jimenez, J. L.: Interpretation of organic components from Positive Matrix Factorization of aerosol mass spectrometric data, Atmos. Chem. Phys., 9, 2891–2918, doi:10.5194/acp-9-2891-2009, 2009. 2673

Ward, Jr., J.: Hierarchical grouping to optimize an objective function, J. Am. Stat. Assoc., 58, 236–244, 1963. 2668

Zhou, L., Kim, E., Hopke, P., Stanier, C., and Pandis, S.: Mining airborne particulate size distribution data by positive matrix factorization, J. Geophys. Res., 110, D07S19, doi:10.1029/2004JD004707, 2005. 2674

ACPD
11, 2655–2696, 2011

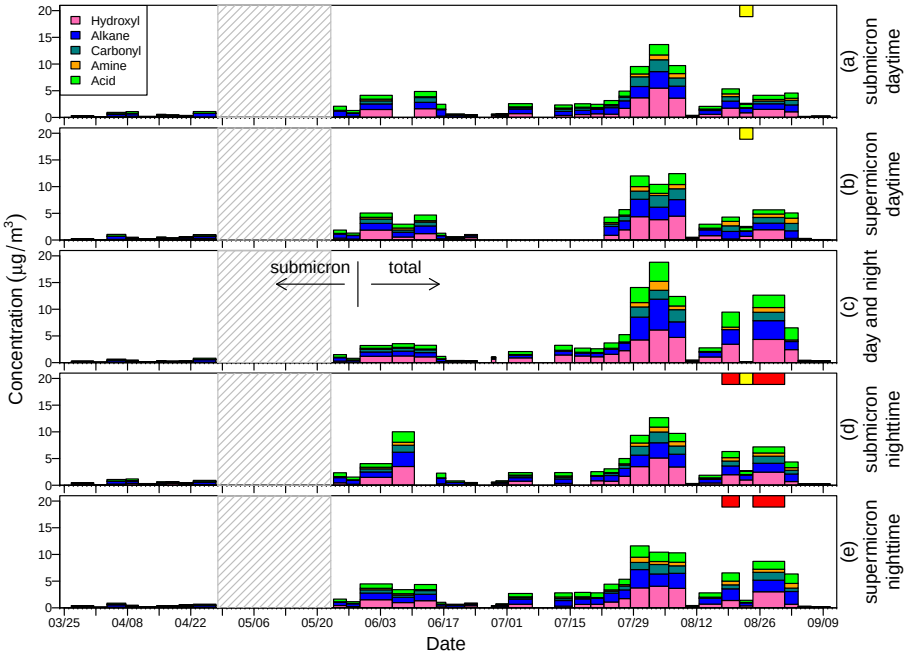

Fig. 1. Time series of OM and OFG as stacked bars: organic hydroxyl (pink), alkane (blue), ketone (teal), amine (orange), acid (green) in **(a)** day submicron, **(b)** day total, **(c)** day and night (submicron before 29 May 2009, and total post that date), **(d)** night submicron and, **(e)** night total aerosol during the 2009 sampling period. The color bar on top shows periods when supermicron aerosol was measured (red) and organosulphate groups were above detection limit (yellow).

ACPD
11, 2655–2696, 2011

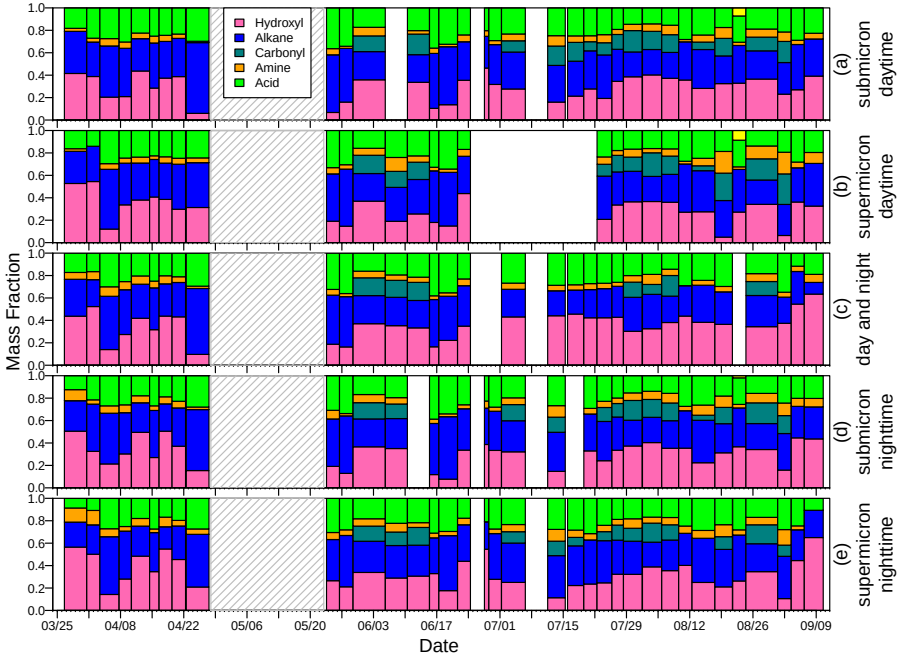

Fig. 2. Time series of OFG fraction as stacked bars with colors as in Fig. 1 (organic hydroxyl (pink), alkane (blue), ketone (teal), amine (orange), acid (green), organosulphate (yellow)) in **(a)** day submicron, **(b)** day total, **(c)** day and night (submicron before 29 May 2009, and total post that date), **(d)** night submicron and, **(e)** night total aerosol for OM above detection limit samples.

ACPD
11, 2655–2696, 2011

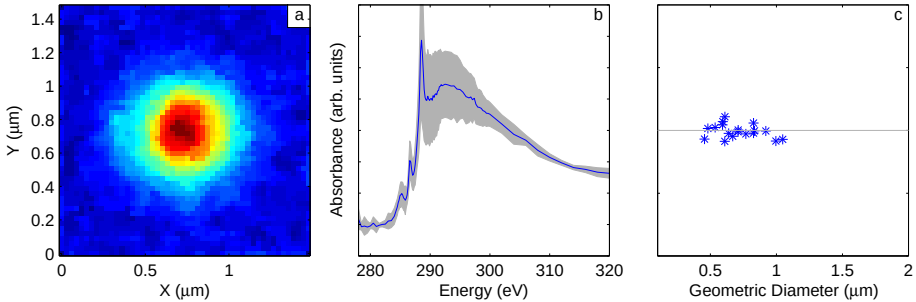

Fig. 3. Images, spectra, and sizes from STXM-NEXAFS analysis. **(a)** Representative absorbance image at 288 electron volts (eV) for particles with absorption at ketone band (286.7 eV). All 18 particles of this type were spherical. **(b)** Average spectra (blue lines)±one standard deviations (grey regions). **(c)** One-dimensional plot showing size and number of particles in used to calculate average and standard deviation of absorbance spectrum (points are randomly jittered along *y*-axis to minimize overlapping of symbols).

ACPD
11, 2655–2696, 2011

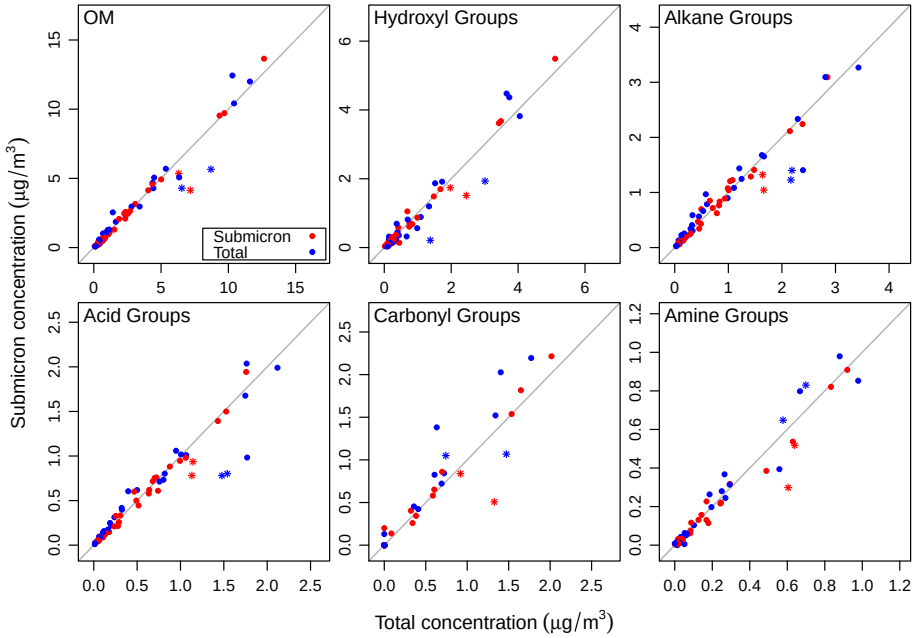

Fig. 4. Comparison between total and submicron sample types by OFG including both day (red) and night (blue) samples. Asterisks label samples with detectable supermicron organic aerosol included in Fig. 5.

ACPD
11, 2655–2696, 2011

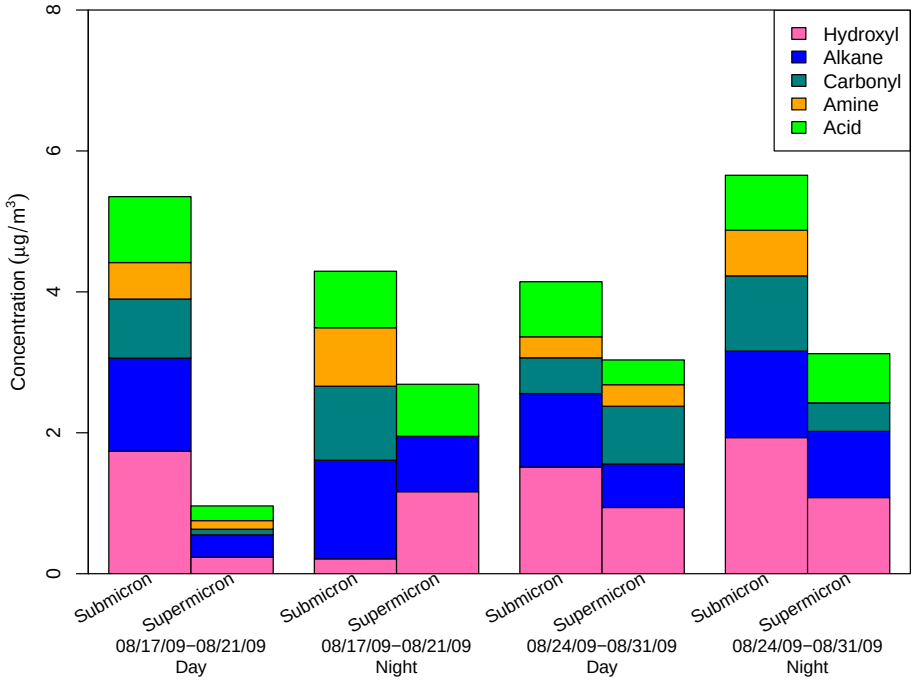

Fig. 5. A comparison between the submicron (left) and supermicron (right) OM and OFG for the periods in which there was a detectable difference between total and submicron samples.

ACPD
11, 2655–2696, 2011

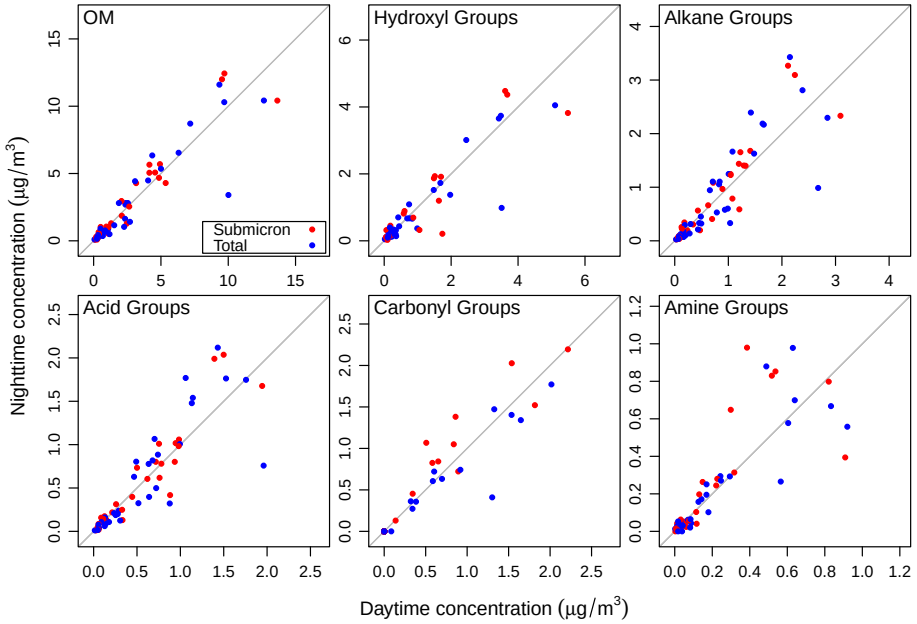

Fig. 6. Comparison between day (06:30 a.m. PST to 06:30 p.m. PST) and night sample types by OFG including both submicron (red) and total (blue) samples.

ACPD
11, 2655–2696, 2011

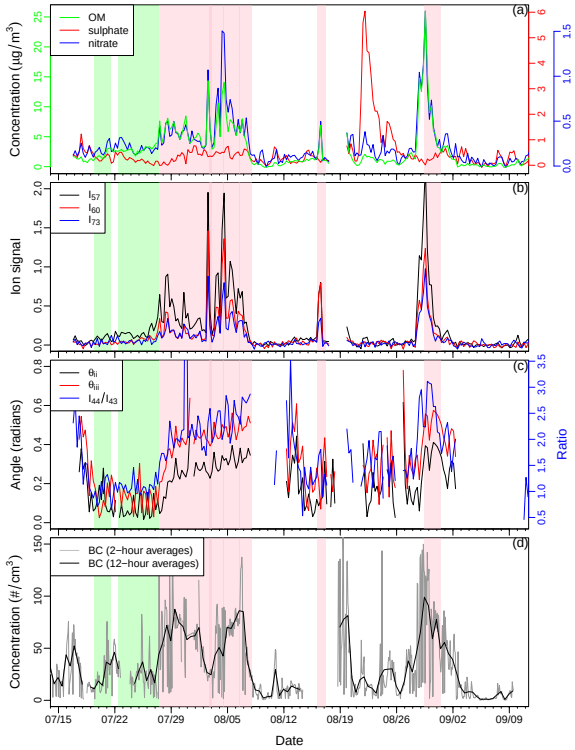

Fig. 7. Time series of co-located measurements of **(a)** ACSM OM, SO_4, and NO_3 mass concentrations, **(b)** ACSM ion signals of *m/z* 57, 60, and 73 mass fragments, **(c)** cosine angle distance of ACSM mass spectra to laboratory spectra from Shilling et al. (2009) and ratio of ion signals of *m/z* 44 to *m/z* 43, and **(d)** BC number concentrations measured by the SP2. Periods during which ACSM OM is below detection limit is removed from panel **(c)**. Pink indicates periods with biomass burning influence, and green indicates periods with primarily non-burning biogenic influence, selected by critera defined in the text.

ACPD
11, 2655–2696, 2011

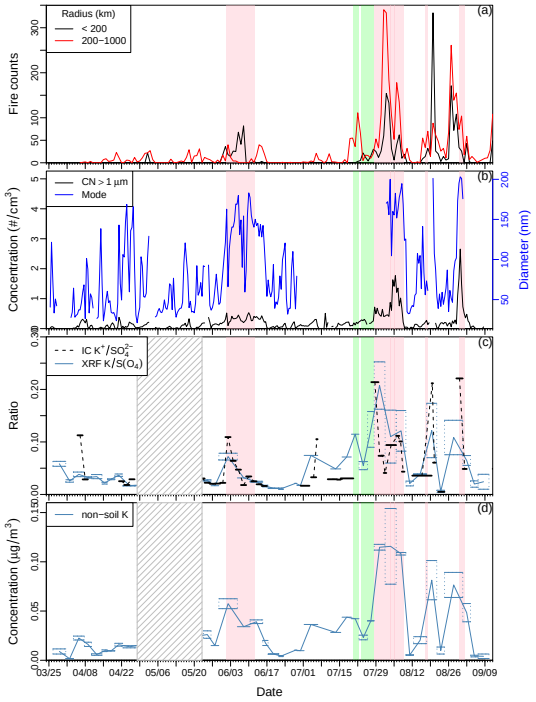

Fig. 8. Time series of **(a)** fire counts, **(b)** supermicron number concentrations and mode of full number size distributions **(c)** potassium to sulphate or equivalent sulphate (all sulphur assumed to be sulphate) ratios measured by IC and XRF, and **(d)** non-soil K calculated from XRF measurements. Boxes for XRF measurements enclose concentrations measured during day and night when both samples were analyzed by XRF. Size distribution modes in **(c)** are from MSP Particle Sizer (prior to 1 July) and TSI SMPS (afterwards). Non-soil K in **(d)** is calculated as $K = R_{soil} Al$, where a value of $R_{soil} = 0.06$ is used (Gilardoni et al., 2009). Pink indicates periods with biomass burning influence, and green indicates periods with primarily non-burning biogenic influence.

ACPD
11, 2655–2696, 2011

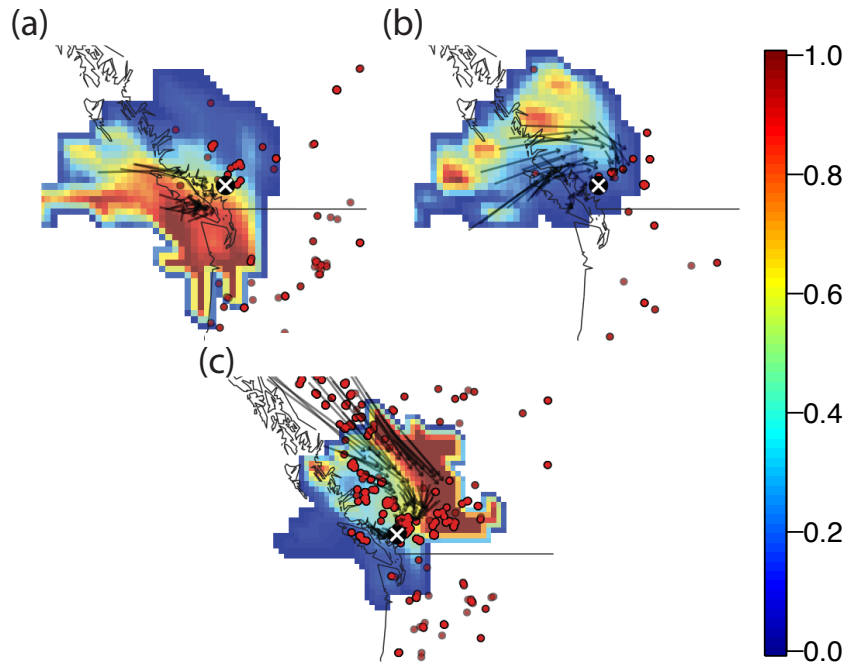

Fig. 9. Potential Source Contribution Function (PSCF) maps shown for **(a)** periods not corresponding to biogenic or biomass burning events (combustion/other), **(b)** periods identified as having been impacted primarily by non-burning forest emissions, and **(c)** periods identified as having been impacted primarily by biomass-burning emissions. Black lines indicate coastline and US-Canadian border. Heat map coloring represents the probability of source contribution (blue=low, red=high) at each location, though for remote sources, warmer (red) colors may only indicate general direction of source. Black arrows indicating wind vectors are superposed (from NOAA HYSPLIT backtrajectory simulations). Whistler Peak measurement site is marked by a white x in each map. Red circles indicate locations of fires by satellite imagery (source: Natural Resources Canada, http://www.nrcan-rncan.gc.ca).

ACPD
11, 2655–2696, 2011

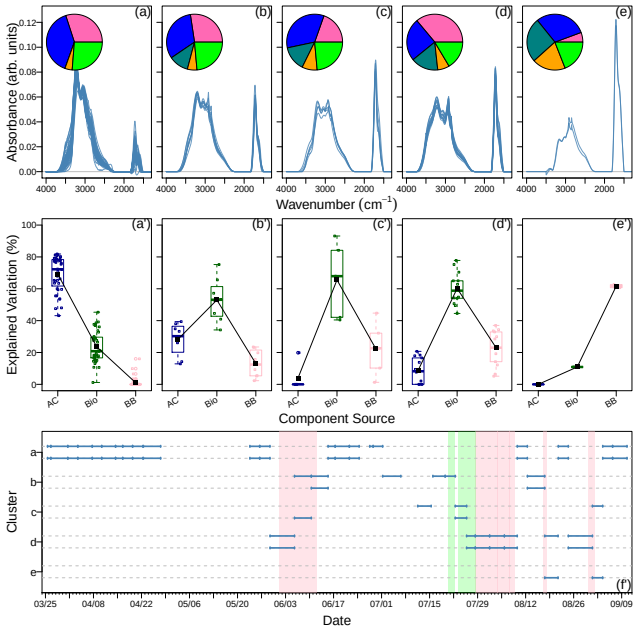

Fig. 10. (a–e) Clustered FTIR spectra of submicron aerosol with inset pie graphs depicting average relative contributions of each functional group to OM: hydroxyl (pink), alkane (blue), acid (green), non-acid carbonyl (teal), and amine (orange) groups. **(a′–e′)** Relative contributions (as Explained Variance) from regression analysis for anthropogenic combustion (AC), biogenic (Bio), and biomass burning (BB) compoments shown as box-and-whisker plots, with individual points overlayed for each category. **(f′)** Time series indicating membership of samples to one of five clusters (labeled on *y*-axis) introduced in top row. Bars horizontally span sampling periods for each filter; positive and negative vertical offsets indicate day or night samples, respectively. Pink indicates periods with biomass burning influence, and green indicates periods with primarily non-burning biogenic influence.

ACPD
11, 2655–2696, 2011

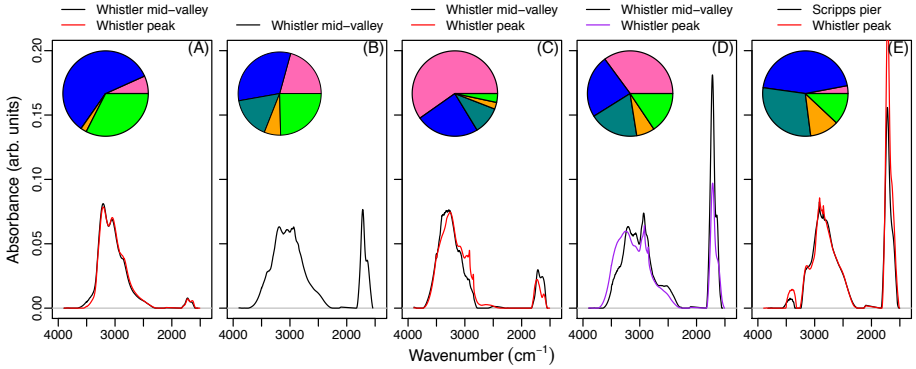

Fig. 11. PMF factors of FTIR spectra from Whistler peak and other studies, with pie graphs showing OFG composition using the color scheme in Fig. 10. **(A)** Combustion factors from Whistler mid-valley (black; R. E. Schwartz et al., 2010) and Whistler peak 3-factor solution (red; nearly identical to 2-factor solution). **(B)** (non-burning) combined biogenic factor from Whistler mid-valley study. **(C)** Biogenic Factor Part 1 from Whistler mid-valley study (black), and Whistler peak Factor Bio (red). **(D)** Biogenic Factor Part 2 from Whistler mid-valley study (black), and Whistler peak forest factor from 2-factor solution (purple). **(E)** biomass burning factor from Scripps Pier study (black; Hawkins and Russell, 2010) in San Diego, CA, and Factor BB from Whistler peak study (red).

ACPD
11, 2655–2696, 2011

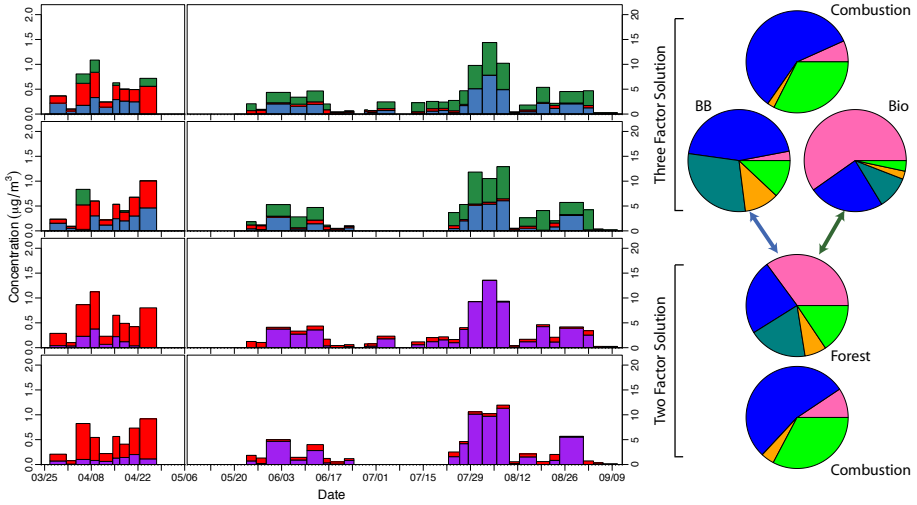

Fig. 12. Time series of submicron OM reconstructed from **(a)** day samples and **(b)** night samples for three-factor PMF with combustion factor (red), Factor Bio (dark green), and Factor BB (blue). Two-factor PMF solution is shown for **(c)** day samples and **(d)** night samples with combustion factor (red) and forest factor (purple). Note the different axis scale for the first and second periods. In the right panel, the OFG composition of the factors are represented with organic hydroxyl (pink), alkane (blue), ketone (teal), amine (orange), and acid (green) groups. Factor BB (left pie) and Factor Bio (right pie) from the three-factor solution are essentially a split of the forest factor from the two-factor solution. Each pie outline color corresponds to the PMF factor in the bar plot.

ACPD
11, 2655–2696, 2011

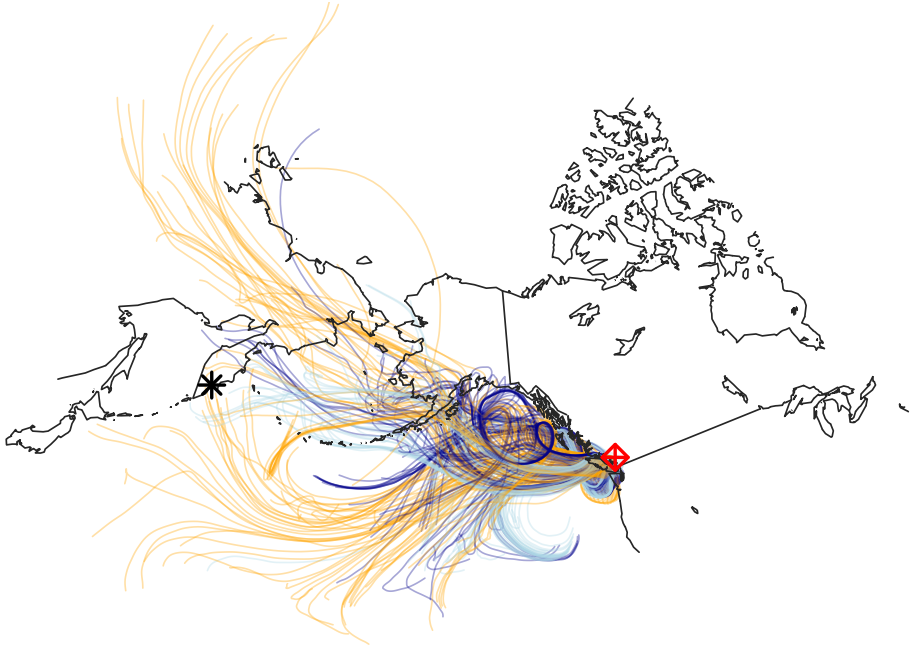

Fig. 13. Seven-day HYSPLIT backtrajectories between 21 August to 24 August colored by initial altitude (AGL): 500 m=dark blue, 1000 m=light blue, 2000 m=orange. Red diamond marks Whistler Peak (at 2182 m); black star marks the location of the Kamchatkan volcano Koryasky.

ACPD
11, 2655–2696, 2011